SLAC – PUB – 3719
June 1985
(I)

X–RADIATION FROM HIGH POWER KLYSTRONS*

FRANK KRIENEN

Stanford Linear Accelerator Center
Stanford University, Stanford, California, 94305

ABSTRACT

Radiation formulas are developed for high power klystrons. The paper deals with energy distributions of:

(*a*) impacting electrons in the collector

(*b*) photons produced by bremsstrahlung

(*c*) photons penetrating the shielding

(*d*) photons crossing the output wave guide

(*e*) the electron background in equilibrium with the photon distribution.

Suggestions are made to improve the shielding in view of reducing adverse effects of x-rays crossing the output wave guide.

Submitted to *Nuclear Instruments and Methods*

* Work supported by the Department of Energy, contract DE – AC03 – 76SF00515.

1. Introduction

The trend to apply ever higher voltages, 400 kV and above, is an incentive to develop radiation formulas, in the first place for safety purposes, and secondly to study adverse effects of x-radiation in the output wave guide.

The principle x-ray source is in the collector and the paper deals with the radiation one would observe outside the collector shielding in a plane halfway the collector and perpendicular to the tube axis.

2. Electrons

Now a fraction of the impacting electrons will have an energy, E_β, higher than the tube voltage E_0. This comes about as the breaking up of the continuous electron beam into bunches cannot be complete: the electrons remaining in between bunches arrive at the gap of the output cavity 180 degrees out of phase and pick up energy from, instead of losing energy to the RF field. The peak to peak gap voltage may be comparable to the accelerating voltage E_0. Hence the energy spectrum $f_1(\hat{E}, E_\beta)$ of the collector electrons has a cut off at $\hat{E} = 2E_0$. The dimension of f_1 will be in $\text{keV}^{-1}\ \text{s}^{-1}$. Although the klystron is pulsed, we will work with average quantities throughout this paper, taking the known duty cycle into account.

The shape of f_1 can be found with a computer simulation [1], or assuming a model for the modulation of the beam current [2]. Figure 1 shows the computer simulation of the SLAC 50 MW klystron, which we take as an example. The pulse voltage is 320 kV, the average current is 0.35 A and duty cycle is 1:1000. We find the normalizing constant C_1 with the relation

$$i_{\text{ave}} = e \cdot \int_0^{\hat{E}} f_1(\hat{E}, E_\beta) \cdot dE_\beta \qquad \text{(A)}$$

where e is the electronic charge, 1.6×10^{-19}C.

The area under the histogram is 3200 keV, hence $C_1 = 6.8 \times 10^{14}$ keV^{-1} s^{-1}. The first moment of f_1 brings out the heat dissipation in the collector

$$W_e = e \cdot \int_0^{\hat{E}} E_\beta \cdot f_1(\hat{E}, E_\beta) \cdot dE_\beta \qquad \text{(kW)}$$

The result, $W_e = 50.8$ kW agrees reasonably well with $W_e = (1 - \eta_{\text{RF}}) \cdot E_0 \cdot i_{\text{ave}}$, in which η_{RF} is the RF efficiency.

A correction is needed on f_1, because the RF drive pulse starts later and ends earlier than the pulse voltage between cathode and anode, so that a fraction of the beam current is not modulated. For the calculation of the radiation the correction has no effect.

3. Bremsstrahlung

The energy distribution $f_2(E_\beta, E_\gamma)$, in keV^{-1}, of bremsstrahlung and characteristic x-radiation of a single electron of energy E_β has the well known triangular continuum with superimposed spikes, which for copper lie in the low energy region and will be ignored.

$$f_2 = C_2 \cdot \left(1 - E_\gamma / E_\beta\right) \ \text{(keV}^{-1}\text{)} \qquad 0 < E_\gamma < E_\beta$$

The constant C_2 is found from the empirical yield formula [3]:

$$\text{yield} = 10^{-6} \times Z \cdot E_\beta = \left(\frac{1}{E_\beta}\right) \cdot \int_0^{E_\beta} E_\gamma \cdot f_2\left(E_\beta, E_\gamma\right) \cdot dE_\gamma = E_\beta \cdot \frac{C_2}{6}$$

where E_β is in keV, $Z = 29$ is the atomic number of copper, hence

$$C_2 \ = \ 6 \times 10^{-6}\, Z \ = \ 1.74 \times 10^{-4} \qquad \text{(keV)}^{-1}$$

Convolution of f_2 with f_1 yields the internal photon spectrum $f_3(\hat{E}, E_\gamma)$

$$f_3(\hat{E}, E_\gamma) = \int_{E_\gamma}^{\hat{E}} dE_\beta \cdot f_1\left(\hat{E}, E_\beta\right) \cdot f_2\left(E_\beta, E_\gamma\right) \ (\mathrm{keV}^{-1}\mathrm{s}^{-1})$$

Figure 2 shows this spectrum, from which we find (graphically) the total number of photons produced inside the collector.

$$\int_0^{\hat{E}} f_3 \cdot dE_\gamma \simeq 2.66 \times 10^{16} \ \mathrm{s}^{-1}$$

The power contained in the photons is given by

$$W_\gamma = e \cdot \int_0^{\hat{E}} E_\gamma \cdot f_3 \cdot dE_\gamma = 0.34 \ \mathrm{kW}$$

The distribution of the power is also shown in fig. 2.

4. Shielding

We look now for the radiation level outside the tube, in a plane perpendicular to the tube axis, half way along the collector body and at a convenient distance, say, 100 cm from the periphery of the tube shielding, see fig. 3. f_3 must actually contain the polar angle, which at the point of observation is about 90 degrees for most of the electrons. Hence we may as well apply a form factor F for this direction, to ease the calculation.

The photon distribution is strongly peaked in the forward direction at high energies, $>$ 200 keV, becomes more isotropic at medium energy and flattens around $\pi/2$ at low energy, $\simeq$ 10 keV [4]. Only the high energy tail of f_3 shows up at P. Figure 4 shows the polar spectrum of 475 keV photons. The mean intensity is a factor 2 above the intensity at 90 degrees, $\cos\phi = 0$. Hence we assume in this calculation $F(\pi/2) = 0.5$.

The calculation of the attenuation $f_4(E_\gamma)$ in the composite shielding, copper collector, water cooling, stainless steel container, lead shielding and a steel mantle is facilitated by the circular symmetry and by the small solid angle the source subtends at the point of observation.

We consider a hollow cylinder of inner radius r and outer radius R and assume the mass absorption coefficient $\eta(E_\gamma)$ of the material in question is known, for instance tabulated [5]. The rays reaching P are about parallel, see fig. 3, so that the path length $L \simeq (R^2 - r^2 \cdot sin^2\theta)^{1/2} - r \cdot cos\theta$ is a simple function of azimuth θ. The attenuation is thus of the type $\int exp\{-\eta(E_\gamma) \cdot L(\theta)\} \cdot d\theta$ which normalized and summed for the various species of absorbing material works out as

$$f_4(E_\gamma) = (2/\pi) \cdot \int_0^{\pi/2} exp\left\{-\sum_i \eta_i(E_\gamma) \cdot L_i(\theta)\right\} \cdot d\theta \qquad \text{(dimensionless)}$$

where

$$L_i = (R_i^2 - r_1^2 \cdot sin^2\theta)^{1/2} - (r_i^2 - r_1^2 \cdot sin^2\theta)^{1/2} \qquad i = 1,2,3,4$$

in which r_i is the inner radius of species i, R_i is the outer radius of species i and r_1 is the inner radius of the collector, where the gamma is born.

The copper collector is grooved externally and surrounded by a stainless steel sleeve. Water cooling is in between. The 2 inch lead shielding is contained by a steel sleeve. The radii are tabulated below:

Table 1

Substance	Cu	SS	Pb	Fe
R_i (mm)	46.06	51.21	109.86	117.48
r_i (mm)	38.48	48.79	51.82	111.23

Note, R_{Cu} is averaged for the grooves and corrected for the equivalent absorption in the water mantle. Figure 5 shows $\log_{10}(f_4)$.

It may be tempting to simplify the calculation of the attenuation, f_4, by assuming a line source in the axis of the tube, so that we obtain $f_4 = exp\{-\sum_i \eta_i(E_\gamma) \cdot (R_i - r_i)\}$, underestimating the shielding power, in our case by a factor 3. Alternatively one could assume an average shielding thickness $L_i = (2/\pi) \cdot \int L(\theta) \cdot d\theta$, overestimating the shielding power, in our case by a factor 2.

The photon distribution at P will be

$$f_5(\widehat{E}, E_\gamma) = \left(F/(4\pi a^2)\right) \cdot f_4(E_\gamma) \cdot f_3(\widehat{E}, E_\gamma) \qquad \left(keV^{-1} \cdot cm^{-2} \cdot s^{-1}\right)$$

where $a = 112\ cm$, the distance from P to the tube axis. Figure 6 shows f_5, assuming $F = 0.5$

5. Radiation

It will be clear that only the high energy tail of the internal photon distribution contributes to the external distribution. We note that if f_5 has the dimension of a flux. The relation of f_5 to the x-ray exposure, x, is found by working out its effect on air. Assuming an air chamber of area A and depth D, the energy flux entering, respectively leaving the chamber:

$$dW_{\text{in}} = dE_\gamma \cdot A \cdot E_\gamma \cdot f_5(E_\gamma) \qquad \left(keV \cdot s^{-1}\right)$$

$$dW_{\text{out}} = dE_\gamma \cdot A \cdot E_\gamma \cdot f_5(E_\gamma) \cdot exp\Big[-\eta_{air}(E_\gamma) \cdot \rho_{air} \cdot D\Big] \qquad \left(keV \cdot s^{-1}\right)$$

Assuming the product between the square brackets, $[\ ] \ll 1$, the absorbed energy

$$dW_{abs} = dE_\gamma \cdot A \cdot E_\gamma \cdot f_5(E_\gamma) \cdot \eta \cdot \rho \cdot D \qquad (keV \cdot s^{-1})$$

The mass of the sensitive volume is $\rho \cdot A \cdot D$ (gram), hence the specific energy loss in air will be:

$$dW_{air} = dE_\gamma \cdot \eta_{air} \cdot E_\gamma \cdot f_5 \qquad (keV \cdot g^{-1} \cdot s^{-1})$$

The exposure in Röntgens is by definition

$$1R = 87.8 \text{ erg/gram} = 5.49 \times 10^{10} keV \cdot g^{-1}$$

hence

$$x = \frac{1}{5.49 \times 10^{10}} \cdot \int_0^{\widehat{E}} dE_\gamma \cdot \eta_{air} \cdot E_\gamma \cdot f_5 \qquad (R \cdot s^{-1})$$

Considering the narrow width of f_5, its FWHM is 40 keV and its mean value is 440 keV we may simplify this integral. The area under $f_5 = 54\ cm^{-2} \cdot s^{-1}$ and $\eta_{air}(440) = 0.0157\ cm^2 \cdot g^{-1}$, hence:

$$x = 0.68 \times 10^{-8} R/s = 0.024\ mR/hour$$

The observed radiation level is usually higher and fluctuates appreciably. This can be understood for reasons set out below.

Only 1/2% of the internal photon production, i.e. the high energy tail around 440 keV, contributes to the external photon flux. In this range the shielding attenuates by a factor 3×10^6. It will be clear that the observed radiation levels are very sensitive to cracks in the shielding or weak spots caused by penetration of cooling pipes, cables, etc. Indeed, the measured background in the klystron test

building is substantially higher than calculated above. Molding and dovetailing the lead shielding parts would improve this. The observed radiation level is also sensitive to the position of the high energy tail of the electrons arriving at the collector. Log f_4, fig. 5, shows that a shift from 450 keV cut off to 500 keV would reduce the attenuation by a factor 10. The position of the tail is presumably related to the tube performance, in particular the RF efficiency. Hence, the x-ray monitor provides a handle on optimization of the tube parameters.

6. Magnetic Shunt

A notorious weak spot is the magnetic shunt, which interrupts the lead shielding, see fig. 7. The local radiation level in the output wave guide is likely to be very high because of the weak shielding. In [6] we suggested that flooding the wave guide with high level x-radiation is a possible cause for window failure.

The weakest passage for the radiation to reach the wave guide occurs in the radial direction and consists of 11 $g \cdot cm^{-2}$ of collector copper, 25 $g \cdot cm^{-2}$ of steel for the magnetic shunt and 6 $g \cdot cm^{-2}$ of wave guide copper. The corresponding attenuation $f_4^{wg} = exp(-17\eta_{Cu} - 25\eta_{Fe})$ is plotted in fig. 8. Assuming uniform source density over the length, h = 50 cm, of the collector, we obtain the photon distribution in the wave guide:

$$f_5^{wg} = (F/(2\pi R_{wg} \cdot h)) \cdot f_4^{wg} \cdot f_3 \qquad keV^{-1} \cdot cm^{-2} \cdot s^{-1} \ ,$$

in which $R_{wg}(= 10\ cm)$ is the radial distance of the wave guide and the polar form factor F = 0.5. This function is plotted in fig. 9. The gamma flux crossing the wave guide is given by:

$$\int f_5^{wg} \cdot d\,E_\gamma \simeq 10^{10} cm^{-2} \cdot s^{-1}$$

7. Seed Electrons

The electron flux traversing the wave guide is in equilibrium with the photon absorption. In the energy range of interest, $200 < E_\gamma < 500$ keV, Compton electrons outnumber photoelectrons in copper by an order of magnitude [7], hence we consider the more abundant process only.

The energy distribution $f_6(E_\gamma, E_\beta)$, in keV^{-1}, of Compton electrons produced by a single photon of energy E_γ, has a cut off at $\widehat{E}_\beta = (2E_\gamma^2)/(mc^2 + 2E_\gamma)$. The distribution is flat for non-relativistic electrons. To simplify matters, we assume that this condition is met, so that we may write, normalizing $\int f_6 \cdot dE_\beta = 1$,

$$f_6(E_\gamma, E_\beta) = \frac{mc^2 + 2E_\gamma}{2E_\gamma^2} \qquad (keV^{-1}) \ , \qquad (0 < E_\beta < \widehat{E}_\beta)$$

Convolution of f_6 with f_5^{wg} yields the energy spectrum of the Compton electrons, $f_7(E_\beta)$. The conversions are proportional to 1 - $exp(-\eta \cdot R) \simeq \eta \cdot R$, where $\eta(E_\gamma)$ is the mass absorption coefficient in copper and $R(E_\beta)$ is the range of the Compton electron in copper, or

$$f_7(E_\beta) = S \cdot \int_{\check{E}}^{\hat{E}} R(E_\beta) \cdot \eta(E_\gamma) \cdot f_6(E_\gamma, E_\beta) \cdot f_5^{wg} \cdot dE_\gamma \qquad (keV^{-1} \cdot cm^{-2} \cdot s^{-1})$$

The lower limit $\check{E} = 1/2E_\beta + (1/4E_\beta^2 + 1/2mc^2 \cdot E_\beta)^{1/2}$, is the cut off mentioned above. $\hat{E}$ is the upper limit of f_5. S is a straggling coefficient. $S = 1/2$ is presumably conservative. $f_7 =$ plotted in fig. 10.

The energy spectrum $f_8(E_\beta, E_\beta^*)$, in keV^{-1}, of a slowing down electron of energy E_β^*, having initial energy E_β, may be convoluted with the Compton spectrum $f_7(E_\beta)$ to yield the energy spectrum $f_9(E_\beta^*)$ of all electrons at all times.

$$f_9(E_\beta^*) = \int_{E_\beta^*}^{\hat{E}} f_7(\hat{E}, E_\beta) \cdot f_8(E_\beta, E_\beta^*) \cdot dE_\beta \qquad (keV^{-1} \cdot cm^{-2} \cdot s^{-1})$$

However f_9 is no longer directional: f_7 is in the forward hemisphere and the multiple coulomb scattering would make the angular distribution in the range of energies concerned about isotropic. Assuming, crudely, that the slowing down is flat, and normalizing $\int f_8 \cdot dE^*_\beta = 1$, $0 \leq E^*_\beta \leq E_\beta : f_8(E_\beta,\ E^*_\beta) = 1/E_\beta$. f_9 is shown in fig. 11. Finally, the number of electrons crossing the wave guide in all directions, which includes the backscatter from the opposite wall of the wave guide:

$$\int_0^{\hat{E}} f_9 \cdot dE^*_\beta = 1.19 \times 10^7 cm^{-2} \cdot s^{-1}$$

This number is presumably subject to large fluctuations, depending on the source distribution in the collector. Appreciable crystal growth has been observed in the neck of the collector of some klystrons, indicative of excessive electron impact and consequently of large radiation in the wave guide. About 100 cm^2 of wave guide area are not well shielded from the collector radiation.

8. Multiplication

A distinctive feature of the seed electrons is its stable phase relation to the RF cycle. Depending on the tube parameters the phase can be right for multipactor, if so, the steady supply assures its continuation. Cyclotron resonance conditions must exist in some parts of the wave guide where the seed electrons originate. This comes about as the cyclotron frequency in the solenoidal magnetic field is slightly above the RF frequency. Hence the wave guide penetration through the magnetic shunt must create some pockets of the right magnitude: $B = \omega_{RF} \cdot m/e = 1018$ gauss. Optimum electron energy for secondary emission is around 1 keV at which the radius of gyration is about 1 mm. The circular motion would favor grazing incidence, enhancing the secondary emission even more. It seems that this mechanism is less voltage sensitive than the pure

RF multipactor. Some autopsied output wave guides show heavy electron impact in the curved part not found in the part beyond the magnetic shunt.

The multipactor in traveling waves moves charges in the direction of the power flow, i.e. in the direction of the RF window, fig. 7. It has been suggested in [6] that charging up of the window causes electrical stress across the ceramic. A sufficiently conducting coating on the window may remove the electric stress but may cause too much joule heating due to RF losses.

It is actually conservation of momentum which drives charged particles in the direction of the power flow. This is easily understood by recalling that the TE10 wave in the wave guide is a superposition of two plane waves propagating under an angle $\pm\alpha$ with the wave guide axis, fig. 12. A charge, initially at rest, would in first approximation move in the direction of the electric field, i.e. perpendicular to the plane of drawing.

The energy E it picks up will be shared among the two plane waves which entails for each of them a momentum loss equal to $E/(2c)$. The vector sum of these two momenta, $p = cos\alpha \cdot E/c$, is the axial momentum acquired by the charge. In the non-relativistic limit we obtain easily $(\dot{z}/c) = 1/2(\cos\alpha) \cdot (\dot{y}/c)^2$, which has always the same sign.

9. CONCLUSION

The radiation level measured outside the tube, in a plane perpendicular to the tube axis, halfway along the collector body at a distance of one meter from the periphery of the tube shielding is convenient to assess the overall shielding requirements. For instance a shift of the high energy tail of the collector electrons by $+50\ keV$ would require an increase of 14 mm of lead to bring the radiation level down to its original value. The electron flux crossing the output wave guide, in equilibrium with the photon absorption, may be reduced by replacing as much copper as possible by uranium. For instance the wave guide wall

facing the collector may be replaced by copper clad uranium of 6 mm thickness. The attenuation, plotted in fig. 8, shows that the radiation level decreases by at least a factor 10. Although somewhat more involved, another order of magnitude may be gained by replacing part of the collector body by uranium. In addition to assuring radiation safety, the radiation monitor is a good diagnostic tool to optimize the tube performance.

10. REFERENCES

1. Hiroshi Yonezawa & Yukio Okesaki. A one-dimensional disk model simulation for klystron design. SLAC-TN-84-5, May 1985.
   K. Eppley *et al.*, Results of simulations of high power klystrons. To be published in IEEE Proceedings 1985 particle Accelerator Conference, Vancouver, B.C., May 1985.
   Simon Yu. Particle-in-cell simulation of high power klystrons. SLAC-AP-34, September 1984.

2. R. Nelson. Theory of x-ray shielding for klystrons. Varian Associates, TMD-42, March 1965.

3. W. Schaaffs. Erzeugung von Röntgenstrahlen. Encyclopedia of Physics XXX, 1 - 77, Springer 1957.
   M. J. Berger and S. M. Seltzer Tables of energy losses and ranges of electrons and positrons. N65-12506, NASA, Washington, D.C., 1964.

4. S. Town Stephenson. The continuum x-ray spectrum. Encyclopedia of Physics XXX. 338-370, Springer 1957.
   W. E. Dance *et al.*, Bremsstrahlung produced in thick aluminium and iron targets by 0.5 and 2.8 MeV electrons. J.A.P. 39 (1968) 2881.

5. G. White Grodstein. X-ray attenuation coefficients from 10 keV to 100 MeV. NBS Circular 583, April 30, 1957.
   E. Storm & H. I. Israel. Photon cross sections from 0.001 - 100 MeV. LA-3753, Los Alamos, November 15, 1967.

6. F. Krienen. Electron wind in strong wave guide fields. SLAC-PUB-3616, to be published in IEEE Proceedings 1985 Particle Accelerator Conference, Vancouver, B.D., May 1985.

7. A. E. Hughes & D. Pooley. Real Solids and Radiation. Wykeham, 1975.
   K. R. Kase & W. R. Nelson. Concepts of radiation dosimetry. Pergamon, 1978.

11. FIGURE CAPTIONS

1. f_1, computer simulation of the energy spectrum of the electrons in the collector.
2. f_3, energy spectrum of the photons inside the collector.
3. Measuring position relative to the collector.
4. Angular distribution of the bremsstrahlung near cut off at 500 keV energy of the electrons in copper.
5. $\log_{10}(f_4)$, attenuation of photon flux in composite collector shielding.
6. f_5, photon energy distribution at one meter from collector shielding.
7. Geometry of the magnetic shunt.
8. $\log_{10}(f_4^{wg})$, attenuation of the photon flux at the wave guide-magnetic shunt intersection. a) as is, b) with 6 mm uranium added.
9. f_5^{wg}, photon energy distribution at the wave guide—magnetic shunt intersection.
10. f_7^{wg}, the equilibrium energy distribution of the Compton electrons at the wave guide-magnetic shunt intersection.
11. f_9, energy spectrum of slowed down Compton electrons at the wave guide-magnetic shunt intersection.
12. Momentum diagram of a TE10 wave.

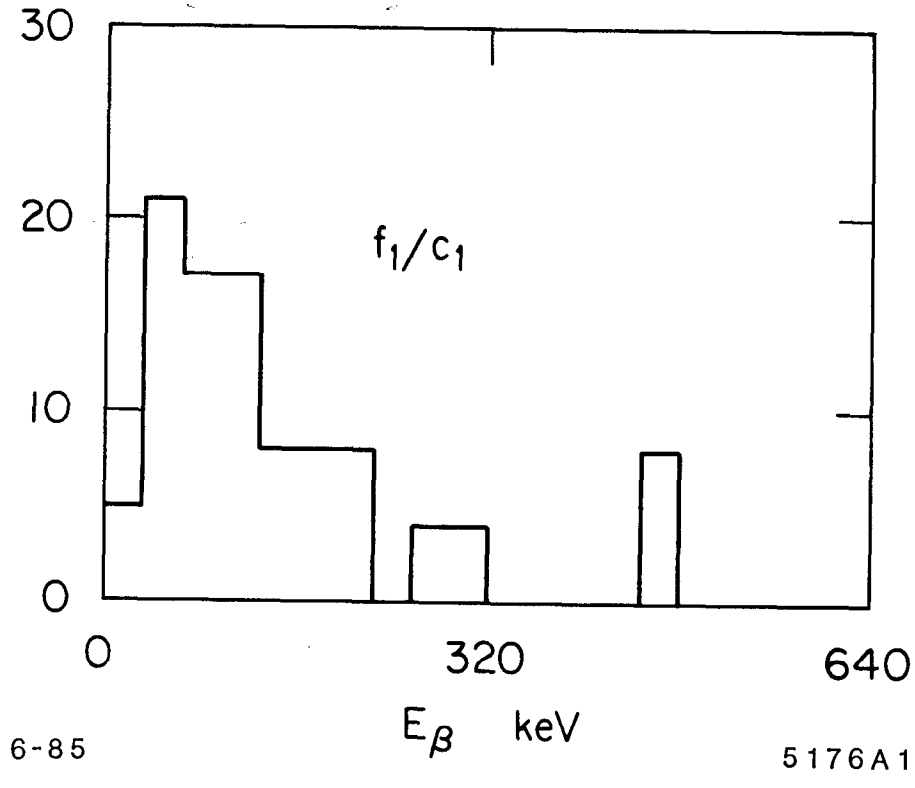

Fig. 1

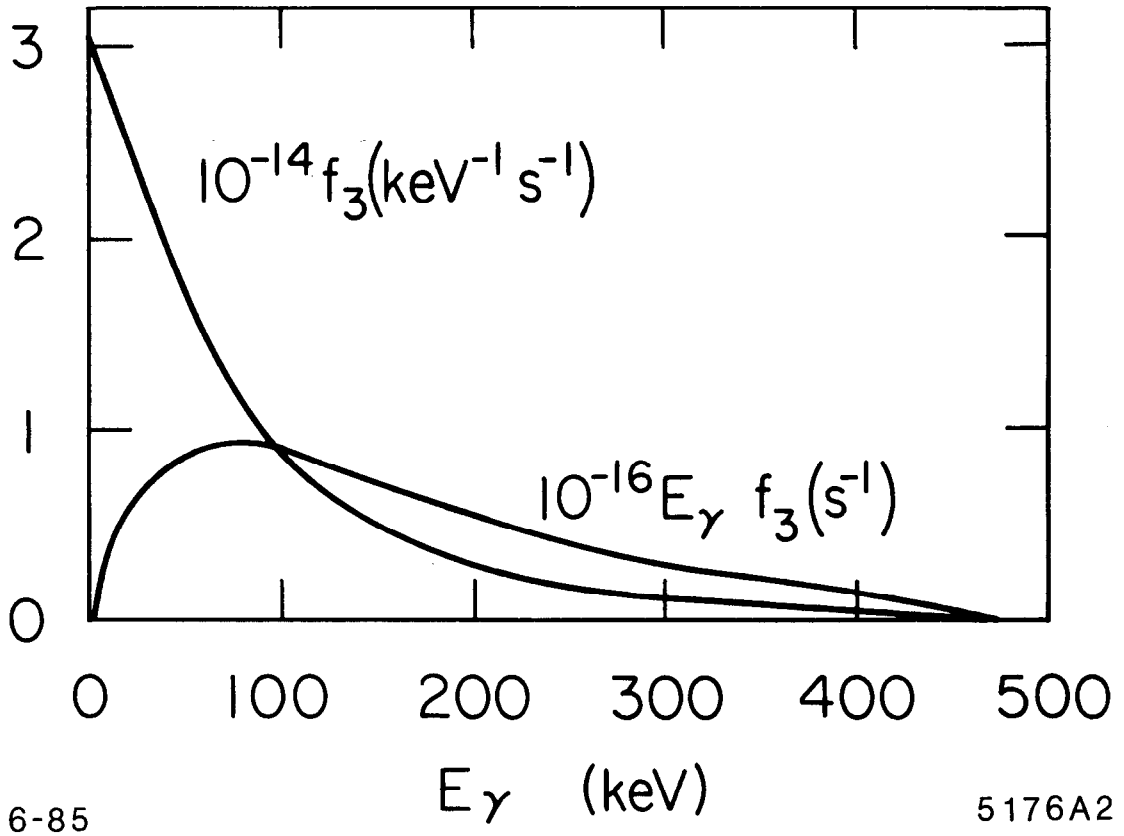
3
2
1
0
$10^{-14} f_3(keV^{-1} s^{-1})$
$10^{-16} E_\gamma f_3(s^{-1})$
0
100
200
300
400
500
E_γ (keV)
6-85
5176A2

Fig. 2

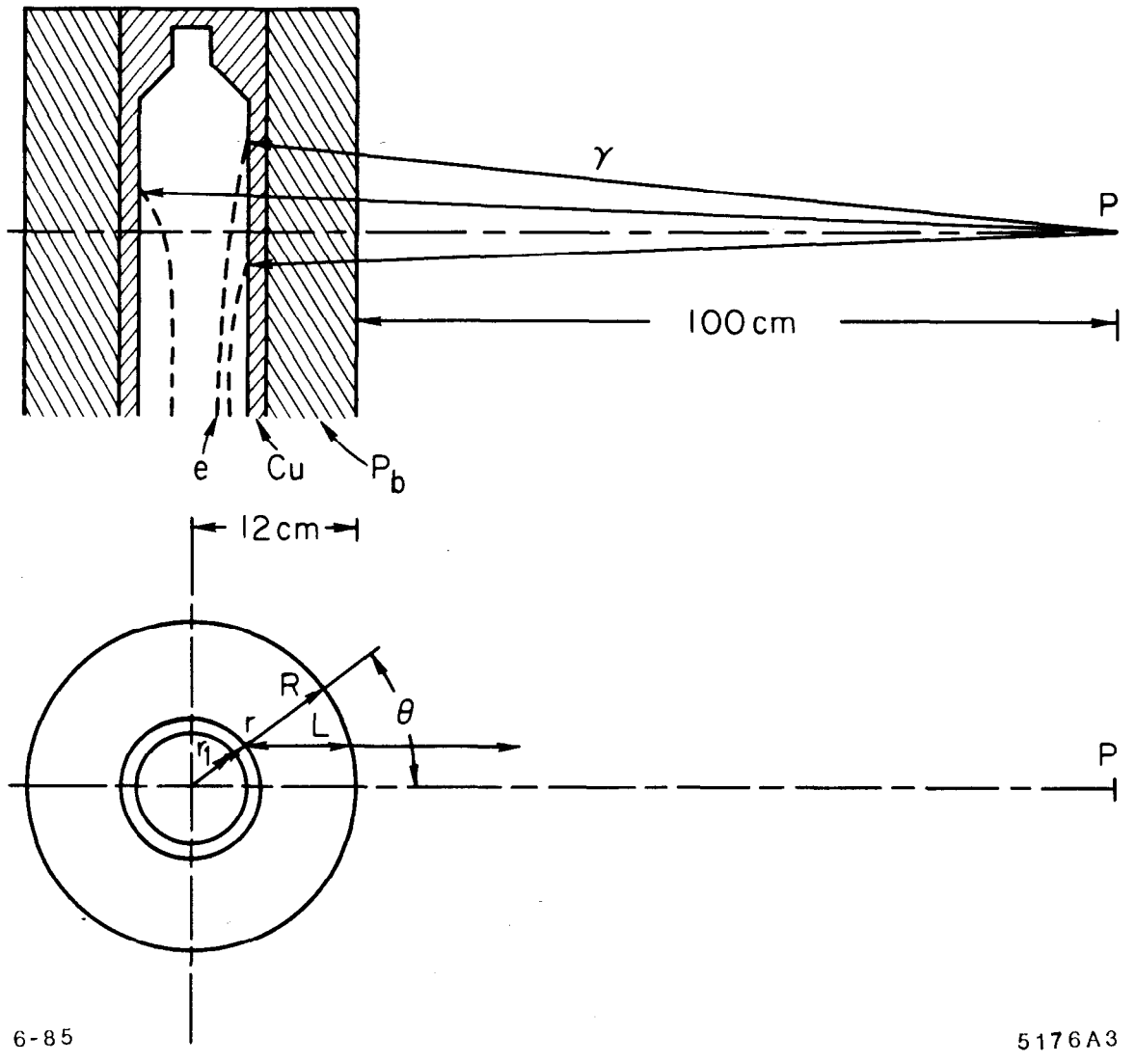

Fig. 3

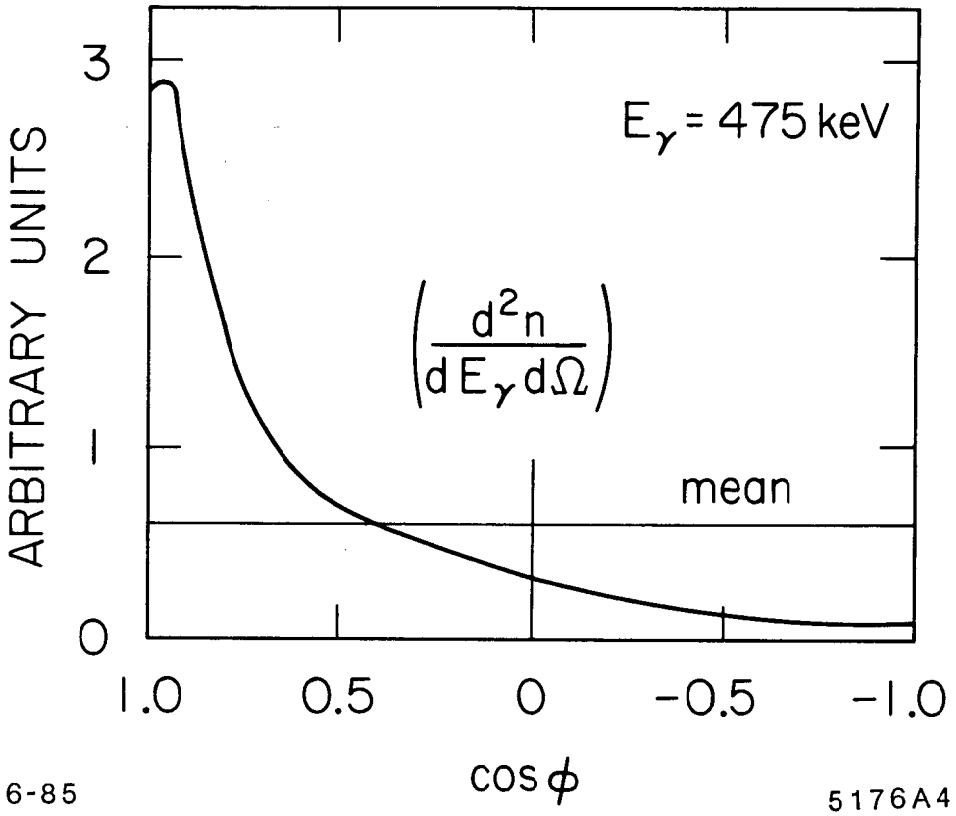
ARBITRARY UNITS
3
2
1
0
E_γ = 475 keV
$\left(\frac{d^2n}{dE_\gamma d\Omega}\right)$
mean
1.0
0.5
0
-0.5
-1.0
cos ϕ
6-85
5176A4

Fig. 4

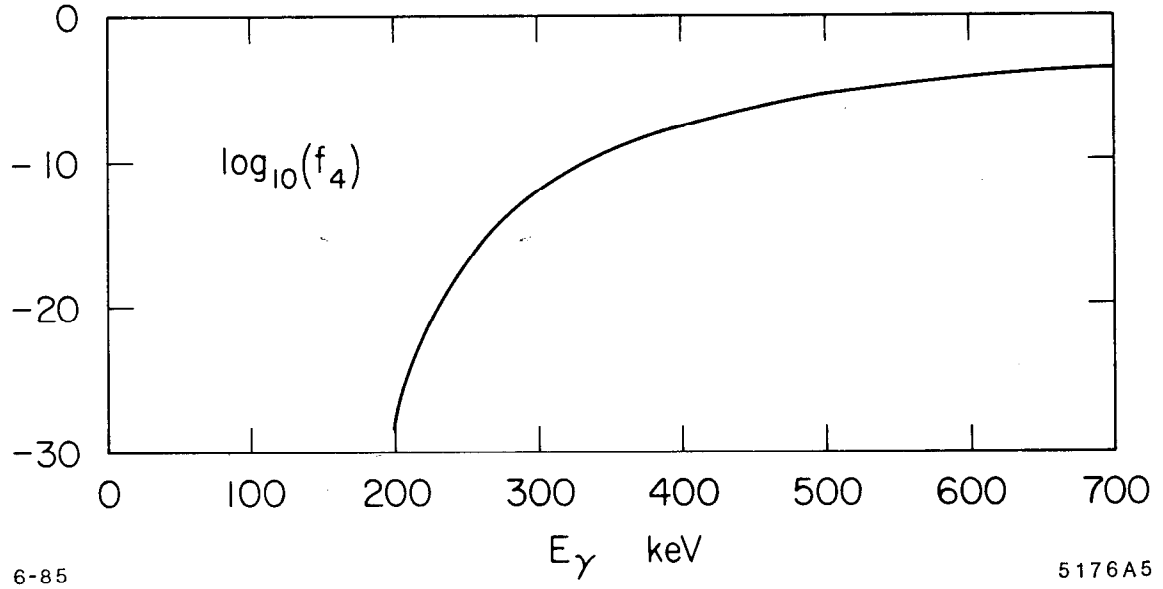
0
-10
-20
-30
$\log_{10}(f_4)$
0
100
200
300
400
500
600
700
E_γ keV
6-85
5176A5

Fig. 5

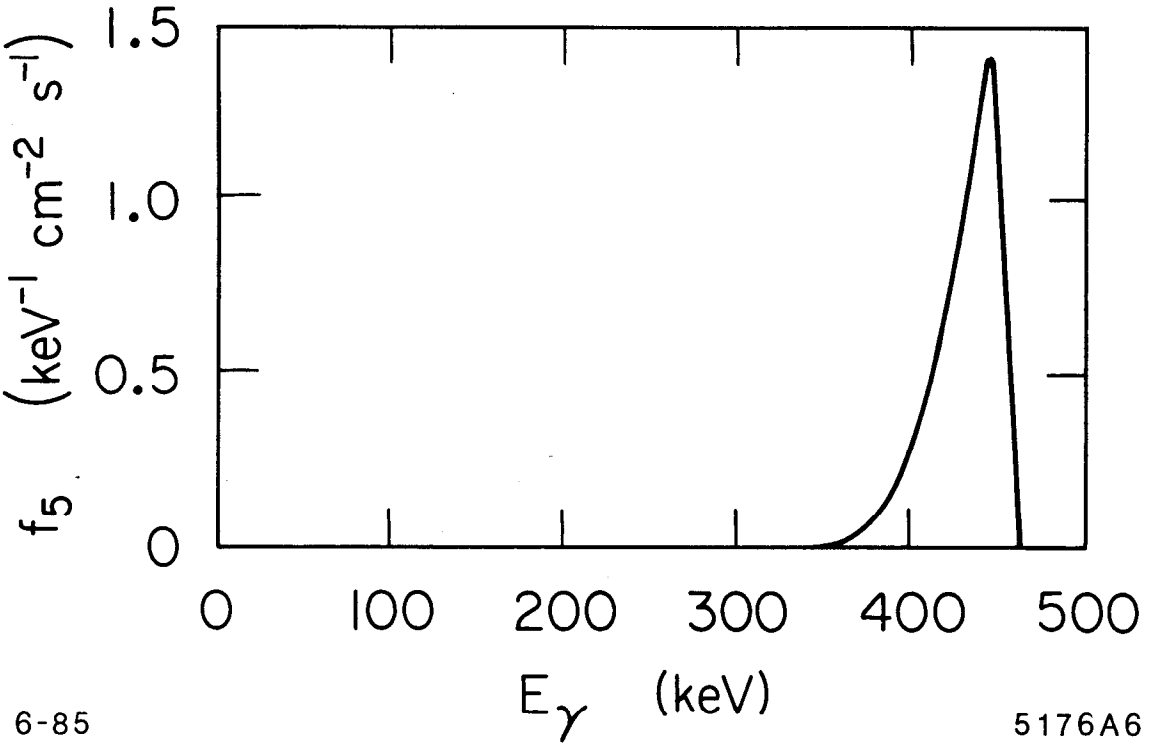
1.5
1.0
0.5
0
f_5 $(keV^{-1}\ cm^{-2}\ s^{-1})$
0
100
200
300
400
500
E_γ (keV)
6-85
5176A6

Fig. 6

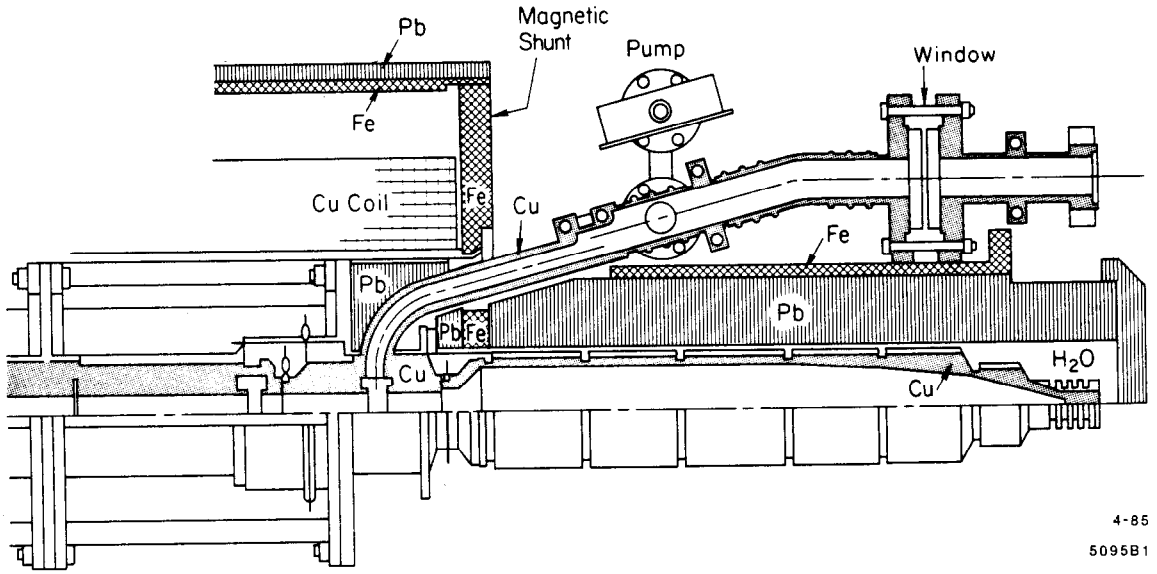
Pb
Magnetic
Shunt
Pump
Window
Fe
Cu Coil
Fe
Cu
Fe
Pb
Pb
Fe
Pb
Cu
Cu
H_2O
4-85
5095B1

Fig. 7

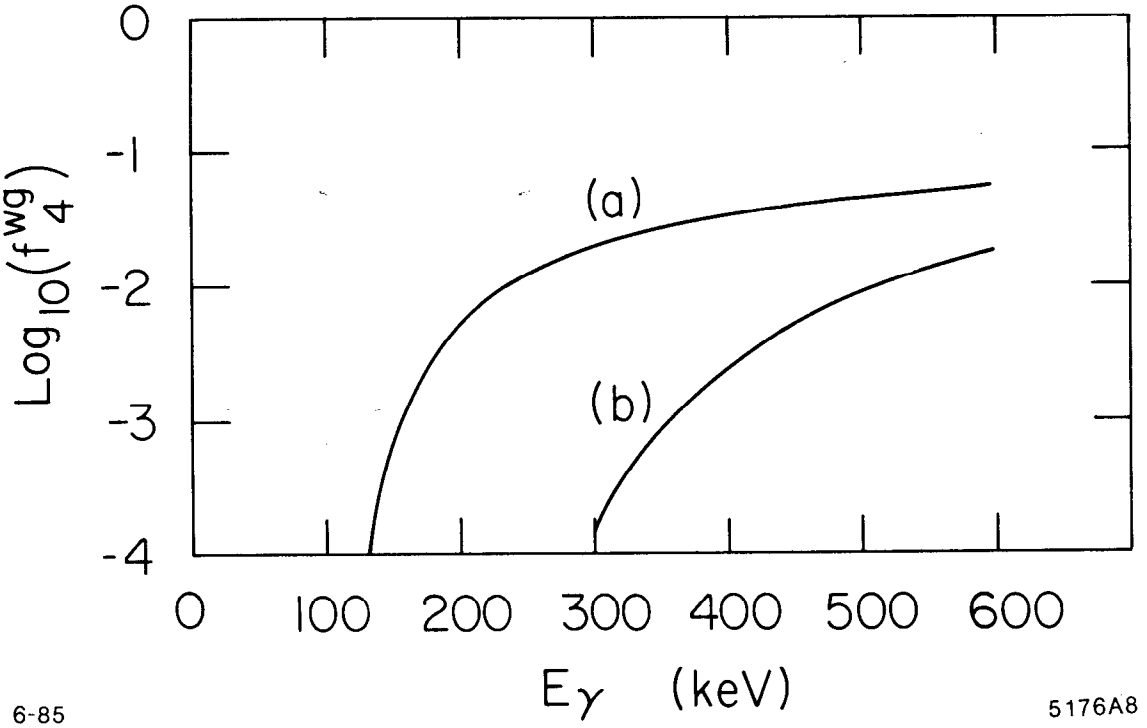
0
-1
-2
-3
-4
$Log_{10}(f_4^{wg})$
(a)
(b)
0
100
200
300
400
500
600
E_γ (keV)
6-85
5176A8

Fig. 8

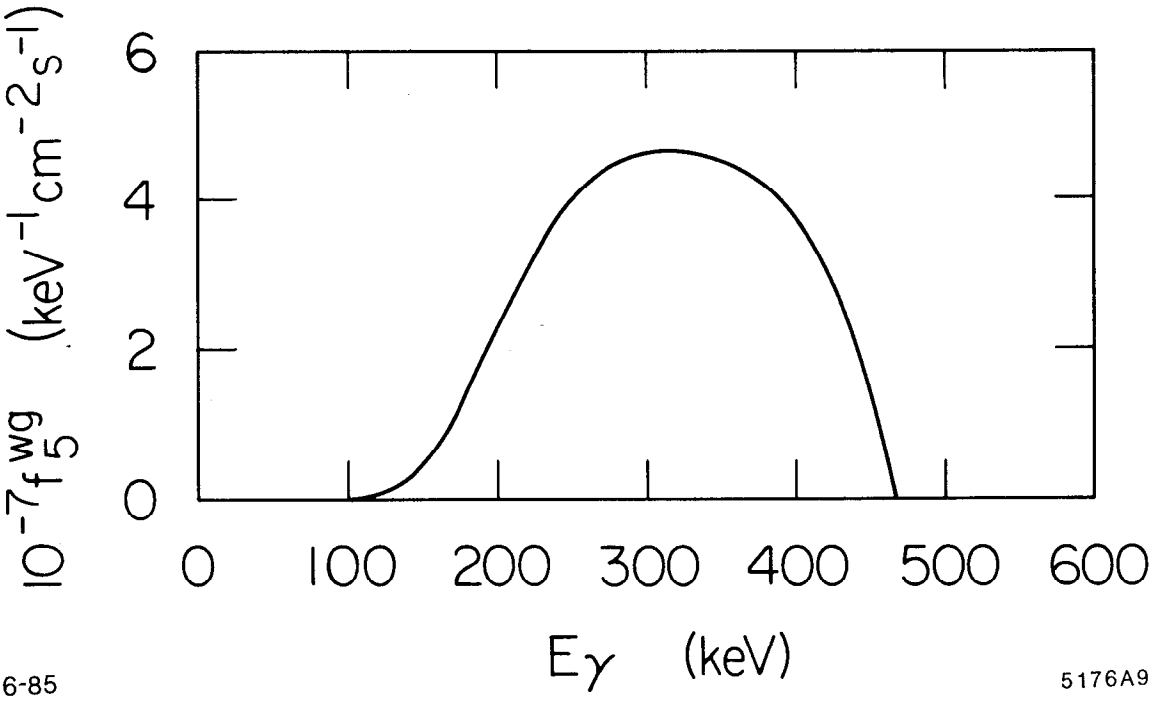
6
4
2
0
$10^{-7} f_5^{wg}$ (keV^{-1}cm^{-2}s^{-1})
0
100
200
300
400
500
600
E_γ (keV)
6-85
5176A9

Fig. 9

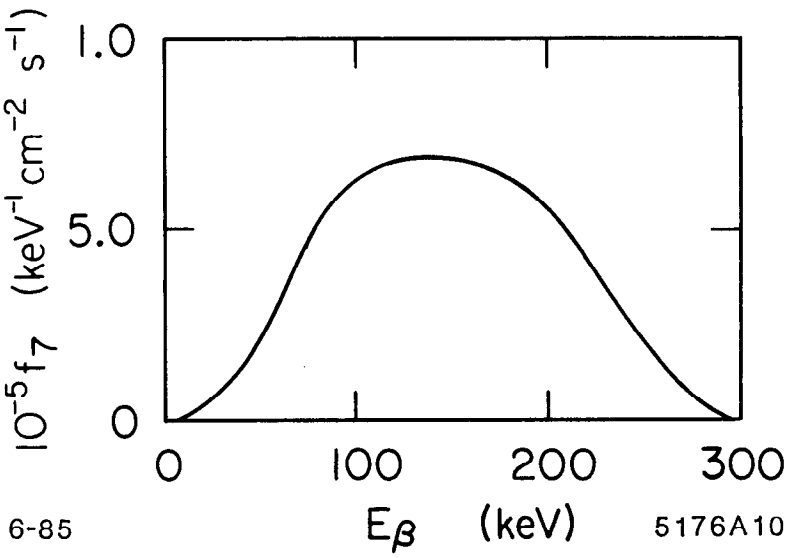

Fig. 10

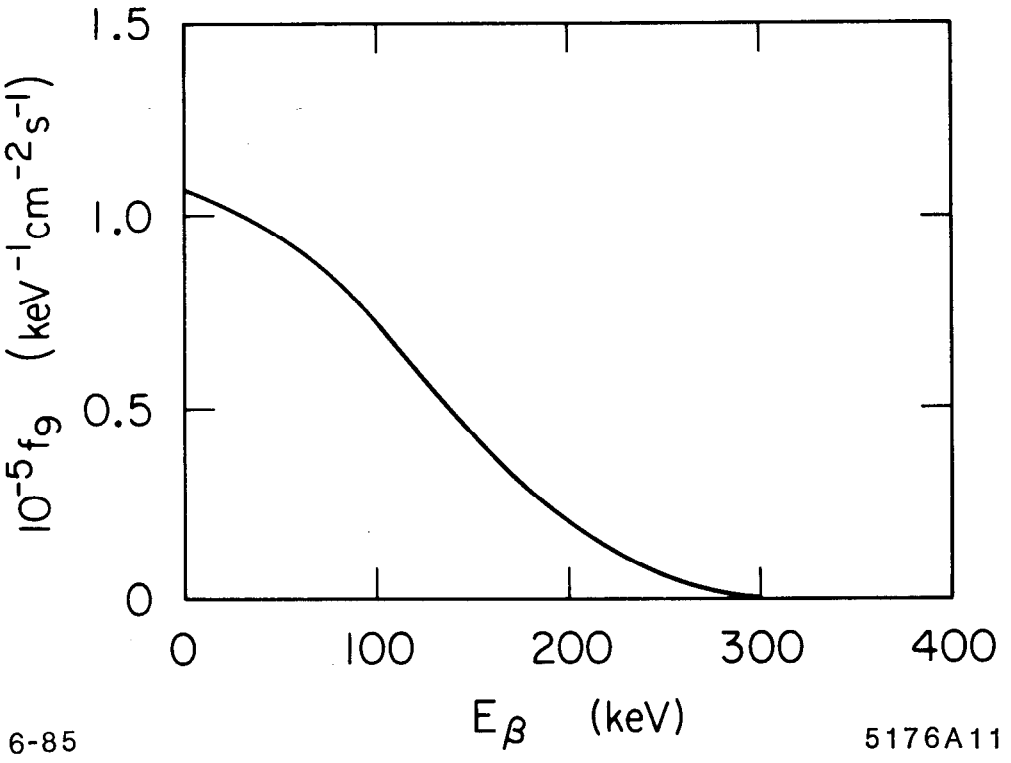
1.5
1.0
0.5
0
$10^{-5} f_9$ (keV^{-1}cm^{-2}s^{-1})
0
100
200
300
400
E_β (keV)
6-85
5176A11

Fig. 11

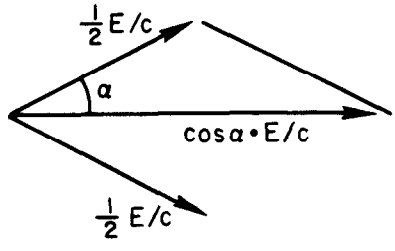

6-85 5176A12

Fig. 12